BMC Complementary Medicine and Therapies

RESEARCH

Open Access

Synergistic effect of curcumin and tamoxifen loaded in pH-responsive gemini surfactant nanoparticles on breast cancer cells

Zeinab Fotouhi Ashin[1], Sanam Sadeghi-Mohammadi[2], Zahra Vaezi[3], Farhood Najafi[4], Shaghayegh AdibAmini[5], Majid Sadeghizadeh[1,6*] and Hossein Naderi-Manesh[1,3*]

Abstract

Background Drug combination therapy is preferred over monotherapy in clinical research to improve therapeutic effects. Developing a new nanodelivery system for cancer drugs can reduce side effects and provide several advantages, including matched pharmacokinetics and potential synergistic activity. This study aimed to examine and determine the efficiency of the gemini surfactants (GSs) as a pH-sensitive polymeric carrier and cell-penetrating agent in cancer cells to achieve dual drug delivery and synergistic effects of curcumin (Cur) combined with tamoxifen citrate (TMX) in the treatment of MCF-7 and MDA-MB-231 human BC cell lines.

Methods The synthesized NPs were self-assembled using a modified nanoprecipitation method. The functional groups and crystalline form of the nanoformulation were examined by Fourier-transform infrared spectroscopy (FTIR), X-ray diffraction (XRD), differential scanning calorimetry (DSC), and dynamic light scattering (DLS) used to assess zeta potential and particle size, and the morphological analysis determined by transmission electron microscopy (TEM). The anticancer effect was evaluated through an in vitro cytotoxicity MTT assay, flow cytometry analysis, and apoptosis analysis performed for mechanism investigation.

Results The tailored NPs were developed with a size of 252.3 ± 24.6 nm and zeta potential of 18.2 ± 4.4 mV capable of crossing the membrane of cancer cells. The drug loading and release efficacy assessment showed that the loading of TMX and Cur were 93.84% ± 1.95% and 90.18% ± 0.56%, respectively. In addition, the drug release was more controlled and slower than the free state. Polymeric nanocarriers improved controlled drug release 72.19 ± 2.72% of Tmx and 55.50 ± 2.86% of Cur were released from the Tmx-Cur-Gs NPs after 72 h at pH = 5.5. This confirms the positive effect of polymeric nanocarriers on the controlled drug release mechanism. moreover, the toxicity test showed that combination-drug delivery was much more greater than single-drug delivery in MCF-7 and MDA-MB-231 cell lines. Cellular imaging showed excellent internalization of TMX-Cur-GS NPs in both MCF-7 and MDA-MB-231 cells and synergistic anticancer effects, with combination indices of 0.561 and 0.353, respectively.

*Correspondence:
Majid Sadeghizadeh
sadeghma@modares.ac.ir
Hossein Naderi-Manesh
naderman@modares.ac.ir

Full list of author information is available at the end of the article

Conclusion The combined drug delivery system had a greater toxic effect on cell lines than single-drug delivery. The synergistic effect of TMX and Cur with decreasing inhibitory concentrations could be a more promising system for BC-targeted therapy using GS NPs.

Keywords Breast cancer, Combination therapy, Curcumin, Drug delivery, Gemini surfactant, Tamoxifen citrate

Background

Breast cancer (BC) is the second leading cause of cancer-related deaths in women, 70% of which belong to the estrogen receptor (ER)-positive BC [1]. Thus, endogenous estrogen-blocking endocrine/hormonal therapies can reduce BC relapse and mortality. Common ER-positive BC treatments include tamoxifen citrate (TMX), letrozole, and fulvestrant [2]. TMX, the first-line endocrine therapy for premenopausal women, blocks the estrogen-signaling pathway by competitive binding to ERs. TMX therapy has several disadvantages, including poor bioavailability and rapid clearance. Long-term TMX therapy causes venous thromboembolism, secondary cancers, central nervous system injuries, and bone growth abnormalities in normal tissues. Long-term TMX therapy induces 20-30% resistance and reduces cancer cell vulnerability, impeding clinical outcomes [3]. Therefore, it is necessary to enhance the therapeutic applications of TMX through a range of approaches, such as increasing target specificity, optimizing therapeutic pharmacokinetics, and reducing dose-dependent toxicity. Compared to standard chemotherapy, specific targeted therapies and nanoscale delivery systems are better choices because of the accumulation of drugs in tumors and reduced side effects, leading to improved tailored treatments [4, 5]. Combination-drug delivery is a common treatment method [6], and polymeric nanocarriers are promising drug delivery mechanisms for combination therapy in cancer treatment [7]. The mPEG2000 urethane gemini surfactants (GSs) are a class of amphiphilic molecules that exhibit biodegradability and are capable of self-assembling into vesicles in aqueous. These molecules have the potential to serve as effective carriers for tumor-specific drug delivery because they can encapsulate 2 distinct therapeutic agents. In addition, they exhibit pH-dependent behavior, thereby enabling their controlled degradation in response to external stimuli [8]. This approach is a remarkably effective method for dispensing drugs within the tumor microenvironment due to a pH gradient [9]. GS represents a viable alternative approach to improve the bioavailability of hydrophobic compounds in specific tissues [10]. The combination of TMX with other natural anticancer components should improve the efficiency of TMX at lower doses [11]. Several bioactive compounds, including schisandrin B (Sch B) [12], β elemene (β-eLe) [13], betulinic acid (BA) [14], quercetin (Que) [15], and curcumin (Cur), have the ability to directly induce apoptosis in tumor cells and decrease their proliferation when used in combination with chemotherapeutic medicines. The utilization of medicinal plant extracts and phytocompounds enhances the effectiveness of antibacterial and antifungal medications. These combinations exhibit greater efficiency and lower toxicity, making them suitable for treating multi-drug-resistant infections [16, 17]. Cur, a flavonoid found in *Curcuma longa*, is a chemical sensitizer used for antioxidant, anti-inflammatory, antibacterial, and drug-resistant tumor treatments [18]. Previous studies have shown that Cur inhibits ER-positive and ER-negative cell growth via dependent or independent pathways [19]. Conventional formulations exhibit poor dispersion and fast omission. Thus, rapid organ removal requires many medicines with side effects [20]. To develop nanocarriers for efficient and safe drug delivery, novel targeted nanomedicine strategies are desirable to increase the tumor site accumulation of anticancer drugs and tissue distribution [21, 22]. Accordingly, this study aimed to examine and determine the efficiency of GS as a cell-penetrating agent in cancer cells to achieve dual drug delivery and synergistic effects of Cur combined with TMX in the treatment of MCF-7 and MDA-MB-231 human BC cell lines. These results will contribute to the development of novel therapeutic regimens for BC patients.

Materials and methods

Materials

TMX (CAS No.: 54965-24-1, purity > 99%), and Cur (CAS No.: 458-37-7, purity of ≥ 99.5%), were purchased from Sigma Aldrich (St Louis, MO, USA). Poly (ethylene glycol) monomethyl ether (mPEG) urethane gemini surfactant were generously provided by the Institute for Color Science and Technology (ICST), Tehran, Iran. Human MCF-7 and MDA-MB-231 cell lines were obtained from Pasteur Institute of Iran (Tehran, Iran). MDA-MB-231 and MCF-7 cells were grown in Dulbecco's Modified Eagle Medium (DMEM)-high glucose (CAT No: 1004760010, Sigma-Aldrich Company, St. Louis, MO, USA) supplemented with 10% v/v fetal bovine serum (CAT Number 16000044; Gibco, USA), and 1% penicillin/streptomycin (CAT No.: 15140122, Gibco, USA). Tetrazolium dye, 3-(4, 5-dimethylthiazol-2-yl)-2, 5-diphenyltetrazolium bromide (CAS No.: 298-93-1), DMSO (CAT No; 5.89569, Sigma, USA), Triton X-100 (CAT No: T8787, Sigma, USA) methanol (CAT No: 1060092500), and all other chemicals and compounds were acquired from Merck (Darmstadt, West

Germany) and were high-performance liquid chromatography (HPLC) grade.

Preparation of nanoparticles

The nanoparticles (NPs) were prepared using a modified nanoprecipitation method [23]. The various formulations, such as GS, Cur-loaded GS (Cur-GS), TMX-loaded GS (TMX-GS), TMX, and Cur co-loaded GS (TMX-Cur-GS) NPs, were self-assembled using a modified nanoprecipitation method (Table 1A). To load TMX and Cur simultaneously, Cur and GS were first dissolved in 3 mL of methanol and then gently added dropwise to TMX in phosphate buffer solution (PBS; pH=7.4) under mild stirring conditions. The ratio of TMX and Cur in TMX-Cur-GS is 1:1 (mg: mg). The solution was then sonicated (Ultrasonic UP200H, Hielscher Ultrasonics GmbH, Germany) at an amplitude of 80% for 2 min (at 30-second intervals) to reach an evenly dispersed solution. Methanol was subsequently evaporated using a rotary evaporator (Heidolph, Germany). The resulting residue was then dispersed in ultrapure water. To remove unencapsulated drugs (Cur and TMX), the dispersion was subjected to centrifugation at 5,000 rpm for 5 min. The unencapsulated Cur and TMX agglomerates (pellet), was discarded, and the NPs formulation (supernatant), containing the encapsulated drugs, was resuspended in ultrapure water. The obtained Cur-GS, TMX-GS, and TMX-Cur-GS vesicles were freeze-dried and stored at 4 °C for subsequent experiments.

Physicochemical characterization of Cur-GS, TMX-GS, and TMX-Cur-GS

The size, polydispersity index (PDI), and zeta potential (ζ) of the NPs were determined using a Zetasizer Nano ZS95 analyzer (Malvern Instruments Ltd., UK) at room temperature [24]. Fourier transform infrared spectroscopy (FTIR) analysis was used to determine the presence of chemical interactions between the drugs (Cur and TMX) and nanocarriers (Bruker, FTIR Tensor 27, Germany). FTIR spectral scanning was performed in the wavenumber range of 400–4000 cm^{-1} on KBr pellet samples [6]. The thermal properties of Cur, TMX, GS NPs, and TMX-Cur-GS NPs were measured by differential scanning calorimetry (DSC; Mettler Toledo 823e, Switzerland). The samples were heated from 0 to 200 °C at a rate of 10 °C • min^{-1}. Thermograms were obtained at a nitrogen gas flow rate of 10 mL/min. The crystallographic characterization of the NPs was determined by X-ray diffraction (XRD) analysis (STOE STRADIVARI, GmbH, Germany) under CuKα radiation (wavelength, 1.5406 Å). The scan rate was adjusted to $3^{o} < 2\theta < 60^{o}$, and the scan angle was 2° • min^{-1}. The morphological features, size distribution, and structure of the samples were studied using transmission electron microscopy (TEM; Zeiss-EM10C,

Table 1 (**A**) size, PDI, and entrapment efficiency of NPs, (**B**) Stability of the freeze-dried TMX-Cur-GSsNPs in PBS (pH:7.4)

(A) Size, PDI, and entrapment efficiency of NPs

Drug: polymer (mg: mg)	Size (nm)	ζ potential (mV)	PDI	EE (%)	LC (%)
GSs					
0:10	328.4 ± 10.01	27.3 ± 4.6	0.32 ± 0.003	-	-
Cur-GSs					
0.5:10	165.6 ± 15.2	6.4 ± 1.3	0.17 ± 0.012	82.2 ± 4.29	2.0 ± 0.41
1:10	200.4 ± 10.2	6.3 ± 1.0	0.21 ± 0.020	87.4 ± 1.74	2.5 ± 0.44
2:10	230.7 ± 17.7	1.9 ± 2.1	0.36 ± 0.008	90.2 ± 0.64	4.9 ± 0.49
TMX-GSs					
0.5:10	216.2 ± 6.7	5.3 ± 1.2	0.39 ± 0.019	81.3 ± 1.77	3.4 ± 0.79
1:10	265.8 ± 15.6	14.9 ± 4.1	0.23 ± 0.007	80.9 ± 3.37	7.4 ± 0.24
2:10	272.2 ± 21.3	16.1 ± 1.3	0.22 ± 0.016	91.2 ± 1.48	8.2 ± 0.62
TMX-Cur-GSs					
0.5:10	241.5 ± 13.6	4.3 ± 13.9	0.27 ± 0.030	Cur:79.04 ± 0.35	2.8 ± 0.79
				TMX:81.8 ± 6.48	4.3 ± 0.67
1:10	246.3 ± 16.1	16.6 ± 7.2	0.38 ± 0.020	Cur:85.1 ± 3.91	3.9 ± 0.44
				TMX:87.1 ± 3.78	5.1 ± 1.10
2:10	252.3 ± 24.6	18.2 ± 4.4	0.19 ± 0.010	Cur:90.1 ± 0.56	4.7 ± 0.33
				TMX:93.8 ± 1.95	6.6 ± 0.55

(B) Stability of the freeze-dried TMX-Cur-GSsNPs in PBS (pH:7.4).

Day	Size (nm)	ζ potential (mV)
1	229.9 ± 10.6	12.2 ± 1.9
7	184.4 ± 10.2	6.0 ± 2.3
14	150.4 ± 7.4	5.8 ± 1.7
30	224.0 ± 14.6	5.2 ± 1.4

Note PDI = Polydispersity Index). EE = Encapsulation efficiency. LC = Loading capacity. and Data are expressed as mean ± SD (n = 3)

Germany) at an acceleration voltage of 100 kV. The diluted aqueous solution of the sample was sonicated for 15 min (Misonix-S3000, USA); in addition, a drop of the sample was placed on a carbon-coated copper grid (300 mesh, EMS, USA) and dried thoroughly at room temperature [6].

Drug content analysis

For the evaluation of the in vitro drug encapsulation efficiency (EE) and drug loading capacity (LC), NPs groups were prepared, and Cur and/or TMX contents in the NPs were measured using a NanoDrop 2000 UV-Vis spectrophotometer (Thermo Scientific, Wilmington, DE, USA). An ultrasonic bath (WiseClean, Germany) was used to dissolve 1 mg of GS, Cur-GS, TMX-GS, and TMX-Cur-GS NPs in 1 mL of the methanol: water ratio (50:50, v/v). The absorbance of the solutions was measured at the maximum absorbance wavelength for TMX (276 nm) and Cur (425 nm). Quantitative analysis was performed using a standard curve of TMX and Cur using UV-Vis spectroscopy to calculate the total amount of encapsulated drug. The encapsulation efficiency and loading capacity were calculated using Eqs. (1) and (2) [9]:

$$\text{Encapsulation efficiency}\,(\%) = \frac{\begin{array}{c}Total\ amount\ of\\ encapsulated\ drug\ \ (mg)\end{array}}{\begin{array}{c}Total\ amount\ of\ drug\\ added\ during\ preparation\ \ (mg)\end{array}} \times 100 \quad (1)$$

$$\text{Loading capacity}\,(\%) = \frac{\begin{array}{c}Total\ amount\ of\\ encapsulated\ drug\ \ (mg)\end{array}}{\begin{array}{c}Total\ amount\ of\\ nanoparticle\ \ (mg)\end{array}} \times 100 \quad (2)$$

Spectroscopy measurements

To demonstrate the encapsulation of Cur in GS NPs, the experiments were performed using an LS-55 fluorescence spectrometer (Perkin Elmer, UK), and the fluorescence spectra were recorded at λ_{em} from 450 to 700 nm (λ_{ex}=425 nm). The free Cur and TMX were dissolved in the methanol: water ratio (50:50, v/v); in addition, their absorption was measured at 425 and 276 nm, respectively, to construct a standard curve to determine the drug loading percentage [8].

Stability of NPs in terms of aggregation and size

The aggregation and size stability of TMX-Cur-GS NPs suspension in PBS (pH=7.4) were determined by monitoring the variation in particle size and zeta potential for 1 month at 4 °C using dynamic light scattering (DLS) measurements.

Drug release profile of NPs

The in vitro release profiles of free Cur, free TMX, Cur-GS, TMX-GS, and TMX-Cur-GS NPs were evaluated in PBS at pH=7.4 and pH=5.5, containing 20% methanol to increase the solubility of Cur in drug release tests. A solution of free drugs encapsulated in NPs (1 mg/mL) was monitored under physiological conditions at 37 °C in a pre-activated dialysis bag (MW cutoff 12 KD). This cutoff was small enough to keep the NPs inside the membrane, but the pores were large enough that they were not a limiting factor for drug release in the dialysate. At predetermined intervals (0.5, 1, 2, 4, 8, 24, 48, and 72 h), the cumulative released was assessed using the standard curve equation [25].

Cell studies

Cytotoxicity assay

MCF-7 and MDA-MB-231 BC cell lines were used to test the effectiveness of TMX, Cur, and dual drug-loaded GS NPs. Both cell lines were cultured in DMEM supplemented with 10% FBS and 1% antibiotic solution (penicillin and streptomycin). Cell viability was measured using a thiazolyl blue tetrazolium bromide (MTT) assay. The MTT assay was performed to investigate the concentration of pharmacologic substances required to induce a 50% mortality rate in the cell population (IC_{50}) [26]. The cells were seeded at a density of 5×10^3 cells/well in 96-well plates and incubated for 24 h. Blank NPs (1–150 µg/mL) were used as controls. In the cytotoxicity assay, the dose of each drug was as follows: for single-drug administration, TMX and Cur was used at a concentration of (0, 1, 5, 10, 25, and 50 µg/mL). Cur and TMX were utilized in co-administration at the same concentrations. When testing NPs containing these drugs, the doses were equivalent to the concentrations used for the free drugs [27].

Cellular uptake analysis

Cur, a biocompatible probe for fluorescence microscopy, was used to monitor NPs uptake into MCF-7 and MDA-MB-231 cells. The intracellular uptake of drug-loaded NPs and free drug solutions was evaluated. MCF-7 and MDA-MB-231 cells were seeded separately in 24-well plates (5×10^4 cells/well^{-1}) for 24 h and then exposed to free Cur, Cur-GS (15 µg/mL), and TMX-Cur-GS (15 µg/mL). The cells were investigated after 3, 6, 9, and 12 h at 37 °C, and DAPI (268298-10MG, Darmstadt, West Germany) solution (10 µg/mL) was used to stain the nuclei. Cell images were taken using an Olympus IX81 inverted fluorescence microscope with a blue filter (Olympus, Hicksville, NY, USA). The acquisition times were typically 120 ms, and the images were captured with an Olympus DP72 digital camera (Olympus, New York, USA) and processed using AnalySIS LS Professional software.

Cell apoptosis analysis

The apoptotic index of Cur-GS, TMX-GS, and TMX-Cur-GS treated cells was determined using flow cytometry and Annexin-V-FLUOS labeling kits (CAT: 55667206, Hoffman-La Roche Ltd., Switzerland). The cells (1×10^5 cells per 12-well plate) were seeded. Cur-GS, TMX-GS, and TMX-Cur-GS NPs were added to the cells and cultured for 48 h at 37 °C. A FACSCalibur flow cytometry device was used to suspend the cell pellets in a solution comprising Annexin, PI, and binding buffer (CAT No: 554781, BD FACSCanto II; BD Biosciences, San Jose, CA, USA). The samples were analyzed using GraphPad Prism version 9.2.1.

Cell cycle analysis

Different cell cycle phases were studied using propidium iodide staining and analyzed using flow cytometry. Briefly, the cells were harvested and washed with PBS, fixed with 70% cold ethanol (CAT No: 1009742500, Darmstadt, West Germany), and incubated overnight at -20 °C. Next, the cells were washed twice in PBS and treated with 50 µL of RNase (CAS No: 9001-99-4, BioBasic, Canada) (100 µg/mL) for 30 min. Then, the cells were washed and stained with propidium iodide (200 µL from 50 µg/mL stock solution, 0.1% Triton X100 in PBS) for 15 min at room temperature. Finally, the cells were analyzed using a BD FACSCalibur flow cytometer (BD Biosciences, San Jose, CA, United States). Different cell cycle phases were determined by FlowJo version 10 (FlowJo LLC, Ashland, OR, USA) [28].

Statistical analysis

The experiment data are presented as mean±SD (n=3–4). Statistical analyses were performed using analysis of variance (ANOVA) and GraphPad Prism version 9.2.1 (GraphPad Software, San Diego, California). P values less than 0.05 were considered statistically significant.

Results

Characterization of nanocarrier and physicochemical properties of TMX-Cur-GS

Measurement of particle size, zeta potential, and polydispersity

The hydrodynamic size distribution and zeta potential of lyophilized NPs were measured using DLS (Fig. 1S). As shown in Table 1A, the highest loading capacity and encapsulation efficiency were observed in all formulations for the drug: polymer ratio (2:10, w/w); this ratio was used for subsequent experiments. Moreover, drug-loaded NPs were substantially smaller than the free GS NPs (328.4±10.01 nm). The average zeta potential of GS NPs was determined to be 27.33±4.63. The findings indicated that the introduction of GS polymer alongside Cur (a negatively charged compound) resulted in a reduction in zeta potential. Specifically, the zeta potential of Cur-GS NPs was measured to be 1.92±2.14. The zeta potential value of the TMX-Cur-GS NPs was 18.2±4.38 mV. The observed reduction in zeta potential could be attributed to the alteration in the polymer aggregation number [29]. The polydispersity index (PDI) of synthetic NPs indicates a monomodal distribution and precise size control with low dispersity [24].

Fourier transform infrared spectroscopy

The FTIR spectra of free TMX, Cur, and TMX-Cur-GS NPs are shown in Fig. 1C. The TMX spectrum showed specific absorption bands at 3028 cm^{-1} (hinting at C–H stretching) and 1732 cm^{-1} related to the C=O stretching bond of citric acid. Notably, these bands were absent in the TMX-GS NPs, suggesting that the drug was entirely encapsulated (Fig. 1A). As shown in Figs. 1A, 2 and 3, the peak at 1602 cm^{-1} was related to the aromatic ring bands observed in both the spectrum of the GS carrier and TMX-GS. In addition, C-H stretching was observed at 2862.9 and 3028 cm^{-1} in both spectra, while the peak at 3028 cm^{-1} in TMX-GS NPs shifted to the 2928 cm^{-1} area, indicating that TMX was loaded in the surfactant. The peak of TMX at 1111 cm^{-1} (C-O-C) was covered by the peak of the carrier and cannot be used to confirm loading. The functional groups of Cur, such as hydroxyl (-OH), carbonyl (C=O), and ethylene groups (C=C), were present at 3405, 1602.1, and 1510.88 cm^{-1}, respectively; in addition, they were characterized in Cur-GS (Figs. 1B and 2). The absence of the 1510.88-cm^{-1} peak in the Cur-GS NPs indicates that Cur is present within the polymeric carrier. In both Cur-GS and TMX-Cur-GS spectra, GS marker peaks, specific peaks at 2924 and 2855 cm^{-1}, and C-N at 1102 cm^{-1} were observed. The characteristic stretching of the C=O citrate group in TMX was not evident in TMX-Cur-GS NPs. Similarly, the peaks associated with the benzene group at 1606 and 1510 cm^{-1} were absent [25, 30]. The FTIR spectra of the TMX-Cur-GS NPs confirmed the presence of TMX and Cur within the nano-polymeric carrier, as well as the formation of hydrogen bonds between the 2 substances. The shifted and broad peak of the phenolic group from 3405 to 3415 cm^{-1} is evidence of hydrogen bond formation in this area [25].

Differential scanning calorimetry

The DSC thermograms of Cur (Figs. 1D, 2, 3 and 4) and TMX (Figs. 1D and 2) demonstrate that TMX and Cur have a sharp melting point of 146.25 °C and 172.57 °C, respectively, indicating their crystallinity [31]. A single endothermic melting peak was obtained for blank NPs at 58.06 °C (Fig. 1D) and for TMX-Cur-GS at 56.97 °C (Figs. 1D, 2 and 3) [32].

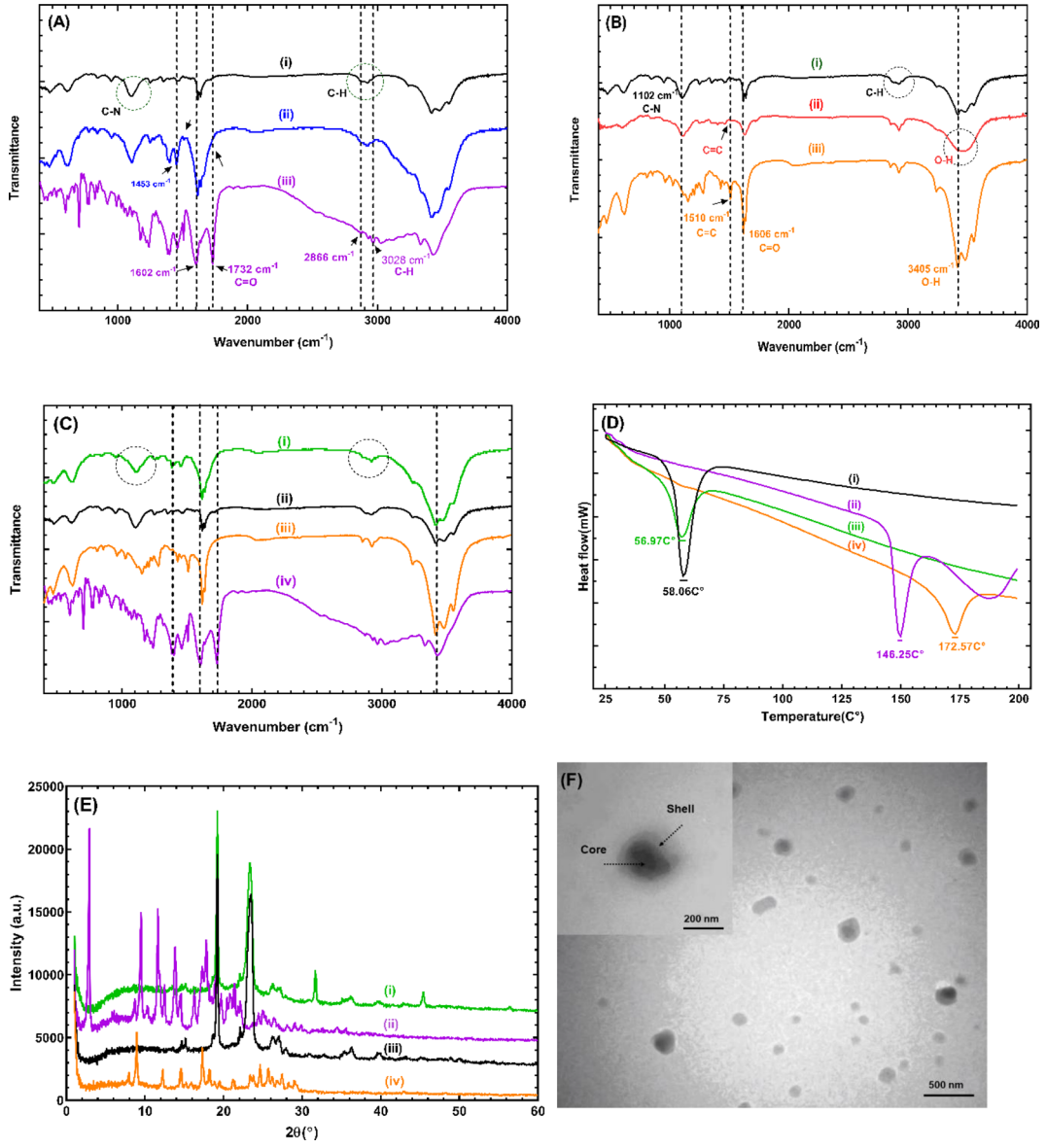

Fig. 1 (**A**) FTIR spectra of GSs (i), TMX-GSs (ii), and TMX (iii), (**B**) FTIR spectra of GSs (i), Cur-GSs (ii), and Cur (iii), (**C**) FTIR spectra of TMX-Cur-GSs (i), GSs (ii) Cur (iii), and TMX (iv), (**D**) DSC thermograms of GSs (i), TMX (ii), TMX-Cur-GSs (iii), Cur (iv), (**E**) X-ray diffraction profile obtained from TMX-Cur-GSs (i), TMX (ii), GSs-NPs (iii), and Cur (iv), (**F**) Transmission Electron Microscopy (TEM) image of TMX-Cur-GSs

X-ray diffraction analysis

The XRD spectra of Cur and TMX contained strong peaks at 2θ scattered angles of 12.28˚, 14.55˚, 17.33˚, and 27.45˚ and 2.91˚, 9.51˚, 13.87˚, and 17.80˚, respectively, indicating that the components were present in the crystalline form. However, these peaks were not observed in the XRD pattern of the TMX-Cur-GS NPs (Fig. 1E). TMX and Cur affected the morphology, size, and crystallinity of GS NPs. According to the XRD results, the crystallinity of the GS NPs was significantly reduced after drug loading, indicating that the drugs were homogeneously incorporated into the polymeric matrix and stabilized in an amorphous state [33].

Transmission electron microscopy

As illustrated in Fig. 1F, the TEM image was used to determine the form of a single vesicle. The spherical structure of the core/shell was disclosed, and the hydrophobic membrane was shown in light gray, whereas the inner core contained water specified by dark gray. The size of the NPs was 167.42±21.02 nm, as determined by ImageJ software. The particle size in DLS measurements was larger than that in TEM because of the hydrodynamic diameter of the particles in the solution [34].

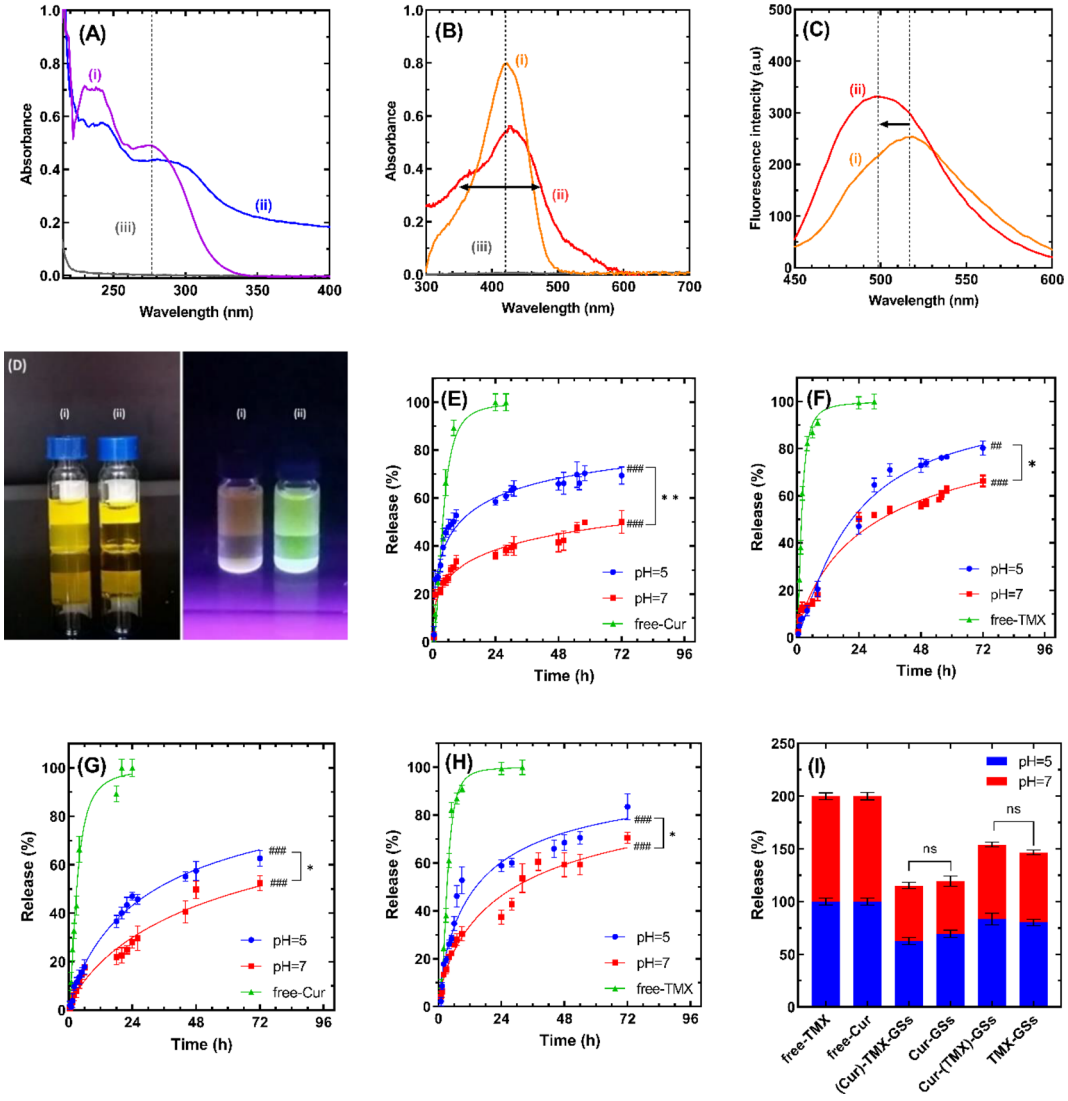

Fig. 2 (**A**) UV–vis spectroscopy analysis of free-TMX (i), TMX-GSs (ii), and GSs (iii), (**B**) free-Cur (i), Cur-GSs (ii), and GSs (iii), (**C**) Fluorescence emission spectra of Cur (i) and Cur-GSs (ii) in an aqueous solution containing 50% methanol excited at 420 nm, (**D**) and bright-field and darkfield photographs of the free-Cur (i) and Cur-GSs (ii), **(E)**in vitro drug release profile of Cur from Cur-GSs, (**F**) TMX from TMX-GSs, (**G**) Cur from TMX-Cur-GSs, (**H**) and TMX from TMX-Cur-**GSs**, (**I**) in PBS at pH 7.4 and pH 5.5. Comparison of drug release percentages after 72 h in PBS at pH 7.4 and pH 5.5. Each data point represents mean ± SD ($n = 3$). ###: P-value < 0.001 and ##: P-value < 0.01 vs. control group (free-Cur, and free-TMX). ns: non-significant, *: P-value < 0.05, and **: P-value < 0.01, vs. each treatment group

Encapsulation efficiency and loading capacity

A formulation with different weight ratios of drug and polymer (w/w) was prepared to evaluate the encapsulation efficiency and loading capacity of NPs through the standard calibration curve for Cur with a linear regression equation of $y=0.0829x+0.0747$, $R^2=0.9929$, and TMX with a linear regression equation of $y=0.02579x+0.04303$, $R^2=0.9941$ (Table 1A and Fig. 2S). The results are given in Table 1A. The unique structure of GS NPs resulted in high encapsulation efficiency (%) and loading capacity (%) values for Cur and TMX. Of particular significance was TMX, which is substantially more water-soluble (10 times) than Cur. Consequently, their values were separately high in the TMX-Cur-GS NPs formulation (2:10). The analysis of drug loading revealed that the increased amount of drug in the formulations led to increased drug loading. This may be due to the ability of the polymer matrix to accommodate a large number of drug molecules in the polymer network before saturation occurs [35]. The saturation point was not determined in the present study.

Steady-state absorption and emission studies

Fluorescence spectroscopy is a robust technique that can be used to examine the interaction between small molecules and macromolecules. This includes the analysis

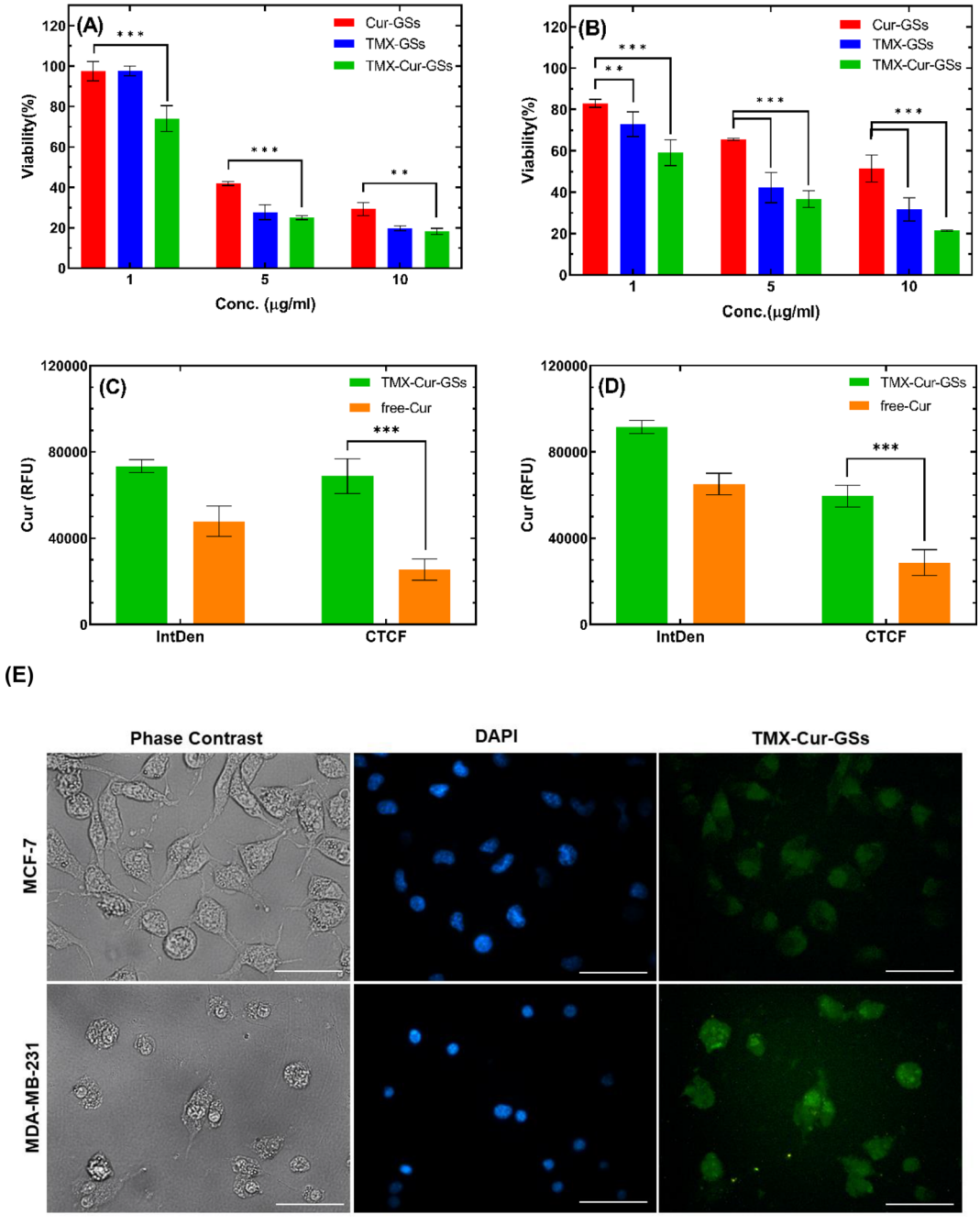

Fig. 3 Synergistic effect of combination NPs (TMX-Cur-GSs) in comparison with individual treatment with TMX (TMX-GSs) or Cur (Cur-GSs) in (**A**) MCF-7 (**B**) and MDA-MB-231 cell lines., Cell uptake and investigation of Corrected total cell fluorescence (CTCF) and Integrated Density (IntDen) after 12 h in both cell lines (**C**) MCF-7 and (**D**) MDA-MB-231, (**E**) intracellular uptake of Cur by MCF-7 and MDA-MB-231 cells at 37oC treated with 15 µg/mL after 6 h (Scale bar 40 µm)

of the binding mechanism, binding mode, and binding constants [36]. The measurement of Cur loading and release kinetics can also be facilitated by this method and the UV spectrophotometric method [37, 38]. The breakdown of Cur and TMX in a buffer reduced their physical properties, while the polarity and pH of the surrounding environment considerably influenced their photophysical properties. However, the presence of polymeric NPs considerably stabilized them under physiological circumstances, and the interaction of medications with the NPs may suppress the degradation under these circumstances. The change in the Cur and TMX absorption spectra seen in the polymeric NPs is proof of this interaction. As shown in Fig. 2A, the absorption spectra of free TMX was 276 nm (Fig. 2A-1); however, the TMX-GS NPs appeared at 291 nm (Fig. 2A). The highest level of

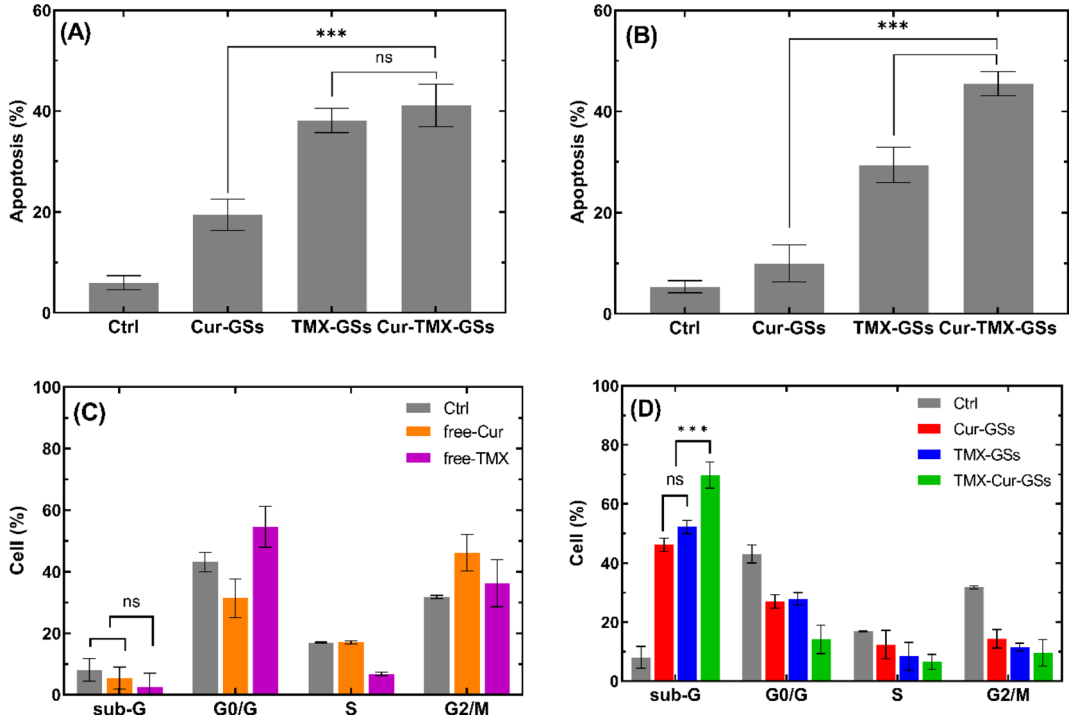

Fig. 4 (**A**) The apoptotic percentage in two cell lines MCF-7, (**B**) and MDA-MB-231 following treatment with combination and single treatment with TMX and Cur for 48 h, measured using Annexin VFITC/PI staining. FITC, fluorescein isothiocyanate; PI, propidium iodide Analysis of apoptosis. Apoptosis is significantly increased by the synergistic effect of TMX and Cur, (**C**) Cell cycle analysis of MCF-7 by Flowcytometry free Drug, (**D**) and drud-loaded nanoparticles. Compared with each other: *:$P<0.05$, **:$P<0.002$ and ***:$P<0.001$

encapsulated Cur's absorption was found to have a similar tendency (a 10-nm blue shift from 425 nm; Fig. 2B). The shoulder peak at 355 nm corresponds to the π–π* transitions in the feruloyl unit, whereas the absorption band near 425 nm corresponds to the lowest π–π* transitions in Cur (Fig. 2B) [31]. The absorption peaks of TMX and Cur loaded in TMX-Cur-GS NPs exhibited bathochromic shifts from the absorption band of the drug solution in the methanol: water ratio and located at 267 and 433 nm, respectively; in addition, the absorption peak intensity also decreased (Fig. 3S). Due to the more viscous structure of the micelle, the Cur incorporated within it displays strong fluorescence in hydrophobic environments. The intermolecular hydrogen interaction between Cur and polymers is likely responsible for the blue shifts in fluorescence [39]. The appearance of an emission peak in water at roughly 498 nm further shows that Cur is sensing a hydrophobic environment inside polymeric NPs (Fig. 2C and D) [31].

Stability of NPs

Table 1B shows the changes in the zeta potential and particle size of the NPs measured within 30 days. As illustrated in Fig. 4S, no significant changes were observed in the size and zeta potential of the NPs. These findings show that TMX-Cur-GS NPs retain structural integrity in a biological context, which is a prominent characteristic of clinical drug carriers. All NPs were stable for 30 days at 4 °C. After 1 month, there was no significant difference in the size or zeta potential of the TMX-Cur-GS NPs ($P<0.0621$) [40].

In vitro drug release

GS is a pH-sensitive polymeric nanocarrier that protonated the GS amine group and expanded the vesicle matrix in an acidic environment, allowing GS NPs to rapidly break down in the acidic environment of tumors (pH 5.6 to 6.8) to release medicines [8]. The release of Cur and TMX from GS NPs under actual physiological (pH=7.4) and acidic (pH=5.5) conditions was demonstrated by their cumulative release profiles from nanocarriers via the dialysis-based assays (Fig. 2E and H). Loading Cur and TMX in GS NPs resulted in prolonged and slowed-down release, which has a significant difference in the release profile of drugs compared to free Cur and free TMX ($P<0.001$; Fig. 2E and F). Cur and TMX release from TMX-Cur-GS was slower and longer than free components due to nanoparticle protection ($P<0.001$; Fig. 2G and H). After 72 h, the sustained release pattern of TMX-Cur-GS displayed a pH-sensitive release profile with a decreasing pH (Fig. 2G and H). It has been shown that 72.19% ± 2.72% of TMX and 55.50% ± 2.86% of Cur were released from the TMX-Cur-GS NPs after 72 h at a pH of 5.5, which is higher than the 58.01% ± 3.00% of TMX and

50% ± 4.65% of Cur released at a pH of 7.4 (Fig. 2I) [41]. GS NPs can release hydrophobic or hydrophilic drugs in different environments. Several parameters during the loading of drugs into NPs can influence drug release, including the ratio, nature, and loading time of drug molecules [42]. Molecules with more polarity exhibit a higher rate of release compared to non-polar molecules. In this regard, Cur exhibited a lower release rate compared to TMX. One of the main challenges encountered in combination therapy is the independent regulation of the release kinetics of drugs. According to Fig. 2I, the TMX-Cur-GS dual-drug system was unaffected by the presence of Cur regarding the TMX release; in addition, no significant difference was observed between the release of TMX alone (TMX-GS) and the combination therapy. Instead, incomplete or inadequately bound molecules on the surface of NPs cause the initial rapid release of TMX or Cur [25]. After the initial burst release, there will be a gradual release of the drug, which is inside the GS NPs and occurs after diffusion, bulk degradation, or both [6]. The results were confirmed using DSC thermograms, in which the changes in the melting point peaks showed that the drugs were most likely in an amorphous form in the matrix.

Cell properties analysis

Cell viability assay

Table 2A shows the MCF-7 and MDA-MB-231 cell survival after treatment with various TMX and Cur formulations. The cell viability measurements revealed that drug composition suppressed cell growth and increased the cytotoxicity in a concentration and time-dependent manner. Also, the GS NPs enhanced the potency of the drug (Figs. 5S and 6S). The IC_{50} is a measure of a drug's efficacy that needs to inhibit a specific biological or biochemical process [43]. The IC_{50} measurements demonstrated that the cytotoxicity effects of Cur and TMX increased by 1.34 and 1.59-fold when loaded into the GS NPs after 72 h (Table 2A). The bioavailability of TMX is typically low due to early metabolism in the intestine or liver, along with its efflux by P-glycoprotein (P-gp). Cur has been identified as a substance that can hinder both the function and expression of P-gp. Therefore, the observed increase in drug efficacy can be attributed to the suppression of P-gp by Cur, which consequently impedes the extrusion of TMX [44]. Drug-loaded NPs had lower IC_{50s} than the free drugs after 48 and 72 h [40]. The low IC_{50} value of Tmx-Cur-GSs means that the components are potent at low concentrations and higher IC_{50} indicate the drugs need to be used in higher dosages [28]. MDA-MB-231 cells showed higher IC_{50} values for free-TMX, TMX-GS, free-Cur, Cur-GS, and TMX-Cur-GS NPs compared to MCF-7 and MDA-MB-231 cells, and all encapsulated nanoparticle treatments showed significant inhibition of MCF-7 cells (Fig. 6S). Cur-GS and TMX-Cur-GS NPs enhanced the cytotoxicity of drugs in accordance with cellular uptake studies. TMX-Cur-GS NPs demonstrated a synergistic effect on BC cells, and a combination index of <1 was found after the treatment of MCF-7 and MDA-MB-231 cells with TMX and Cur after 72 h (Table 2B). As shown in Fig. 3A, B and a synergistic effect was observed in TMX-Cur-GS NPs compared to TMX-GS and Cur-GS NPs for 72 h in both BC cell lines, and statistical analysis was performed based on 2-way ANOVA.

Cellular uptake assay

Studying cellular absorption plays a critical role in understanding the mechanisms by which TMX-Cur-GS interacts with cells, the location of its encapsulated material

Table 2 (**A**) IC_{50} of TMX, Cur, TMX-Cur, TMX-GSs NPs, Cur-GSs NPs, and TMX-Cur-GSs NPs upon treatment with MCF-7 and MDA-MB-231 cells, (**B**) combination index of TMX and cur (TMX-Cur-GSs NPs) on cell survival

(A) IC_{50} of TMX, Cur, TMX-Cur, TMX-GSs, Cur-GSs, and TMX-Cur-GSs upon treatment with MCF-7 and MDA-MB-231 cells.

Cell lines	MCF-7			MDA-MB-231		
	24 h	48 h	72 h	24 h	48 h	72 h
Cur	18.86 ± 0.65	8.10 ± 0.39	7.09 ± 0.76	21.44 ± 0.74	20.16 ± 0.87	17.32 ± 1.47
Cur-GSs	17.14 ± 0.37	5.35 ± 0.84	5.26 ± 0.71	20.32 ± 0.51	10.84 ± 0.77	9.25 ± 0.56
TMX	10.69 ± 0.59	7.15 ± 0.81	5.72 ± 0.62	17.20 ± 0.72	8.64 ± 0.46	8.18 ± 0.67
TMX-GSs	10.13 ± 0.76	5.69 ± 0.63	3.59 ± 0.55	12.00 ± 0.64	4.66 ± 0.52	3.69 ± 0.47
TMX-Cur	15.75 ± 0.52	8.55 ± 0.56	4.86 ± 0.58	28.69 ± 0.91	9.09 ± 1.67	4.96 ± 0.62
TMX-Cur-GSs	12.38 ± 0.77	6.72 ± 0.45	2.34 ± 0.32	27.02 ± 0.58	7.57 ± 0.34	1.72 ± 0.26

(B) Combination index of TMX and Cur (TMX-Cur-GSs NPs) on cell survival.

Cell lines	CI		
	24 h	48 h	72 h
MCF-7	1.021	1.211	0.561
MDA-MB-231	1.882	1.254	0.353

Note Data are the mean SEM of at least three independent experiments, The combination index (CI) of the combined effect of TMX and Cur on cell survival was analyzed. The synergistic action of Cur and TMX was identified based on the CI theorem of Chou–Talalay [35], additive effect (CI = 1), synergism (CI < 1), and antagonism (CI > 1) in drug combinations). CI: combination index

inside the cell, and the amount of TMX-Cur-GS ingested. Fluorescence microscopy was used to quantitatively evaluate the cellular uptake of Cur. As shown in Fig. 7S, the accumulation of Cur in cells was time-dependent, between 3 and 12 h of incubation with free-Cur and TMX-Cur-GS. Moreover, the Cur retention time in the cell during the 12-h incubation showed a broader cytoplasmic distribution of TMX-Cur-GS compared to free Cur (green fluorescence), while the blue fluorescence was associated with nuclei stained with DAPI (Fig. 3E). As illustrated in Fig. 3, the fluorescence intensity in each of the cell populations of MCF-7 (Fig. 3C) and MDA-MB-231 (Fig. 3D) was evaluated using ImageJ software, and the entrance of the drug into the cells was compared with each other through the corrected total cell fluorescence (CTCF) and integrated density (IntDen) after 12 h. As shown in Fig. 3E, taking advantage of the autofluorescence of Cur, strong fluorescence was observed in cells incubated with Cur-GS and TMX-Cur-GS after 6 h of treatment. It has been indicated that encapsulated Cur gained more efficient entry into the cells than free Cur, along with a time-dependent increase in the cellular uptake of Cur, which is consistent with previous studies [45].

Cell apoptosis assay

TMX and Cur alone or in combination promoted apoptosis in MDA-MB-231 and MCF-7 cells compared with controls (Fig. 4, and 8 S). According to these findings, TMX-GS is more effective than Cur-GS in inducing cell death in BC cells. In addition, as shown in Fig. 4A and B, the apoptosis values increased in the presence of the combined TMX and Cur in both MCF-7 and MDA-MB-231 cells: 44% of MCF-7 cells and 48% of MDA-MB-231 cells. TMX kills BC cells more effectively with this combination therapy. TMX suppresses the mitogenic action and proliferation of estrogen by competing with ERs. It induces cancer cell death by modulating protein kinases C, TGF-β, and p53 [46, 47].

Cell cycle analysisDrug-loaded GS NPs inhibited cell proliferation and promoted apoptosis. Flow cytometry was performed to check for cell cycle arrest in MCF-7 cells stimulated with free drugs and drug-loaded NPs (Fig. 4, and 9 S). Treatment of MCF-7 cells with free drug and Cur-GS, TMX-GS, and TMX-Cur-GS at concentrations lower than the IC_{50} revealed accumulation in the fraction of cells in Sub-G1 phases (apoptosis) and reduced S and G2 cell populations, indicating a pause in cell cycle and promoting apoptosis (Fig. 4D). TMX-Cur-GS, which included TMX and Cur (5 µg/mL), was able to kill almost 70% of MCF-7 cells. However, the same quantities of TMX and Cur alone did not show this effect, and the cellular distributions did not differ significantly from control levels in the G1, S, or G2 phases (Fig. 4C S).

Discussion

The synergistic combination of two or more therapeutic drugs is a promising strategy to overcome the adverse toxicity and other side effects that inhibit the efficacy of many treatments. Various natural plant-based compounds and extracts have anti-tumoral characteristics, which could be valuable in improving new anti-cancer NPs [48]. Several research indicates that natural products significantly treat a wide range of human diseases, including many types of cancer [49]. Studies have proven that combining natural bioactive components and chemotherapeutic agents makes a synergistic antitumor impact through many mechanisms, such as inducing apoptosis in tumor cells, suppressing tumor cell proliferation, and inhibiting tumor multidrug resistance (MDR) [16, 50]. Researchers indicate co-delivery of Cur with PTX leads to an improved therapeutic outcome in the treatment of human cervical cancer. This effect is mediated through the NF-κB-p53-caspase-3 pathway [51], and studies show Cur was employed without and in conjunction with TMX in order to mitigate tamoxifen-resistance in cancer cells. Cur reverses many resistance mechanisms established by tamoxifen-resistant cells. It modulates the altered pathways including MAPK, PI3K/Akt, C-myc, Cyclin D, NF-kB, and SRC, hence restoring sensitivity to TMX in tamoxifen-resistant cells [52].

The findings of this study suggest that drug-loaded GS NPs form tighter structures and have a positive surface charge. The size reduction can be attributed to the lipophilic compound, which has the potential to act as a bilayer stabilizing agent [53], leading to a greater loading capacity. For nanomedical applications, the preferential size is ≤200 nm, and our data showed that the average particle size of Tmx-Cur-GSs is 252.3±24.6 nm with a narrow size distribution (PDI 0.19). According to other studies, encapsulation of Cur and piperine within the zein NPs with a coating of ι-carrageenan molecules shows the average size of the CPZC NPs was 408.8±3.1 nm [54], and the average size of Cur- and 5-fluorouracil-loaded NPs was less than 200 nm [27]. Lipid-polymer hybrid NPs co-encapsulated Cur and cisplatin and the nanoparticle size was 225 nm with 0.21 PDI [55]. The co-loaded of TMX and docetaxel in the polymeric nanoparticle depict a 213 nm diameter and 0.26 PDI [40]. The particle size and PDI of co-loaded TMX and quercetin in Tmx-QT-NPs were 185.3±1.20 and 0.14, respectively. To decrease the size of the droplets, Tmx-QT-NPs prepeared by probe sonication for 60 s [56]. Co-delivery of TMX and imatinib by temperature-sensitive liposomes indicats the average particle size under 200 nm and PDI<0.4. to obtain this size and PDI, the synthesized NPs were sonicated for 3 min and extruded [30]. Literature indicates that nanomaterials within the range of 100–300 nm have demonstrated efficacy in evading the liver and spleen,

organs responsible for nanoparticle metabolism, and decreasing their circulation duration. The shape and surface properties of particles are also important factors, as they enable precise targeting of certain cells [57]. The size of NPs can be altered by modifying solution conditions, polymer concentration, production techniques, drug loading, and drug release mechanisms [58]. A low PDI indicates that the sample has a narrow distribution of particles, which is desirable. In contrast, a high PDI (up to 1) can lead to a mixture of NPs with varying loading capacities, reduced physical stability, and distinct release profiles [59]. Our investigations confirm the monomodal distribution, and our results about average particle size align with the other studies.

The ability to form hydrogen bonds may contribute to the stability of NPs, thereby enhancing their viability as drug delivery systems. The addition of TMX and Cur to the GS NPs altered their physical properties and increased their thermal stability. Despite the change in the physical properties of GS NPs after the addition of drugs, the results confirm that the combination of drug molecules is feasible and that they can also alter the photophysical properties [60]. Photophysical findings suggest that Cur possesses both hydrophilic aryl and hydrophobic diketone groups, which may interact with polymeric NPs that are both van der Waals and electrostatic [44, 61]. The mechanisms of release from a gemini polymer include a combination of erosion and diffusion [32]. The gradual degradation of the polymer matrix in the release medium could explain the sustained drug release pattern of both medicines for 72 h. Interestingly, the cumulative release of Cur was much less than that of TMX at all times, which is related to its stronger affinity to the hydrophobic polymer matrix, which has a higher tendency to release in media than Cur, facilitating its rapid release [56]. The co-administration of TMX with anticancer agents can yield an additive or synergistic effect, resulting in the inhibition of cancer cell proliferation. Strategic co-administration of anticancer drugs promises more effective therapy for ER-positive BC than monotherapy. Promoting cell death is a highly successful strategy for preventing the uncontrolled growth of cancer cells. Researchers have shown that the IC_{50} value for Cur and TMX in dendrosome OA400 was under 5 μg/mL at 72 h [28]. In this research our experimental results, Tmx and Cur demonstrate significant antitumor and potentialy reduce the required dosage and minimize adverse effects of cytotoxic therapies as the IC_{50} was 2.34 μg/mL at 72 h.

A significant increase in cytotoxicity and reduction in medication dosage can be attributed to the heightened ability of the treatment to penetrate, undergo endocytosis, and exhibit enhanced adherence to cancer cells because of the zeta potential. TMX-GS NPs enter the cell through endocytosis and are not targeted by P-gp pumps; thus, TMX remains in the cell for a longer time and induces apoptosis via protein kinase C suppression, causing higher cytotoxicity [62]. TMX and Cur exert their effects on distinct downstream signaling pathways, ultimately resulting in the induction of apoptosis in cancer cells. Combined treatment with TMX and Cur resulted in elevated Bax and decreased Bcl2 expression in both MCF-7 and MDA-MB-231 cells. These findings indicate an increased rate of apoptosis and synergistic effects [27, 63, 64]. Concurrent administration of TMX and Cur demonstrated a synergistic effect, leading to a subsequent decrease in the required dosage of TMX. Consequently, this reduction in dosage mitigates the associated side effects of TMX. In addition, the same result was demonstrated in the combined treatment with TMX and concanavalin [65], as well as with Cur and temozolomide [66]. Cur induces a strong antiproliferative effect on the binding activity of NF-κB when protein kinases and tumor-promoting pathways are inhibited [67, 68]. These results confirm the hypothesis that Cur exerts an inverse effect on the growth of ER-negative cells more efficiently than ER-positive cells and that Cur and TMX together have a more significant effect on stopping the development of both ER-positive and ER-negative cells [19], with endocytic cellular uptake as the main mechanism in MCF-7 cells. The transported positive charge of NPs increases cellular absorption and leads to increased accumulation of Cur in cells due to the enhanced cellular uptake of Cur NPs, thus causing cytotoxicity and apoptosis [69]. Combination therapy is more effective in inducing cell death in BC cells because TMX competitively binds to the ER and modulates signaling proteins (such as protein kinase C, TGF-β, and p53) to induce cancer cell apoptosis; in addition, Cur increases pro-apoptotic proteins, such as Bax expression. In combination therapy, necrosis occurs because of the high-dose toxicity of drugs [28]. Cell cycle and apoptosis studies in MCF-7 cells revealed that TMX-Cur-GS NPs induced apoptosis and increased the population of cells with DNA content in the sub-G1 phase. Combining Cur and TMX induces apoptosis in cancer cells. These results are similar to those of other studies, wherein treatment with TMX and Cur caused cell cycle arrest at the sub-G1 phase [28]. In addition, treatment with TMX caused a cell cycle pause in the G1 phase, whereas treatment with Cur resulted in cell death by stopping cells in the G1/S and G2/M phases and activating the caspase-3 pathway [69, 70]. Cell cycle arrest is not the mechanism by which TMX reduces cell viability. The pH-responsive polymeric nanocarriers have been developed by utilizing the acidic milieu within tumor tissues and tumor cell /lysosomes to facilitate the effective and prompt release of anticancer drugs into tumors [71]. A novel approach was employed to

create pH-sensitive NPs for the simultaneous administration of DOX and Cur. This was achieved by synthesizing self-assembled amphiphilic macromolecular prodrugs. Cur-DOX-NPs were well taken up by cells, and they were specifically delivered to the MCF-7 cell line, where they had strong cytotoxic effects [72]. A pH-responsive micelle system was designed for the co-delivery of PTX and Cur. This system enhances their cellular absorption and allows for deep penetration into tumors. Additionally, it causes a burst release of PTX and Cur. These benefits also contributed to the optimal effectiveness of the combined PTX and Cur treatment [73]. In this study, the pH responsiveness of the NPs is primarily attributed to the GSs incorporated in their structure. GSs is a type of surfactant that consists of two hydrophobic tails and two hydrophilic head groups connected by a spacer. This unique structure allows GSs to exhibit different behaviors under varying pH conditions due to the ionizable nature of its hydrophilic head groups. GSs have demonstrated pH-responsive characteristics due to the protonation of urethane bonds in acidic pH, which makes them highly attractive for drug delivery applications. This protonation increases the hydrophilicity of the GSs, causing the NPs to swell and become more soluble [74]. Our results are in line with previous studies, the GSs showed an increase in the cellular uptake of BC cell lines that can be caused by endocytic cellular uptake, then the accumulation of Cur and Tmx in cells increased, thus causing cytotoxicity and apoptosis. We suggested that GSs play a crucial role as a pH-responsive nanocarriers and have the ability to transfer two different therapeutic components simultaneously.

Conclusion

Co-administration of TMX and Cur led to increased cytotoxicity and apoptosis in BC cells, demonstrating synergistic effects. The incorporation of drugs into the polymer matrix results in improved internalization and uptake by cancer cells, thereby reducing the required dosages and minimizing adverse effects. The combined treatment exhibited contrasting effects on the proliferation of cells expressing ERs, both positive and negative. In general, the use of GS NPs as carriers for drug delivery exhibited enhanced efficacy compared to unbound drugs, thereby underscoring their potential to enhance the efficacy of cancer treatment. Further studies are necessary to investigate the potential clinical relevance and enduring effects of this combined therapeutic approach.

Supplementary Information

The online version contains supplementary material available at https://doi.org/10.1186/s12906-024-04631-x.

Supplementary Material 1

Acknowledgements

We are very grateful to Professor Saman Hosseinkhani for his helpful comments on the manuscript and Mr. Reza Mahdavian for assistance with in vitro experiments.

Author contributions

The study was designed by Z.F.A and M.S. All experiments were conducted by Z.F.A. Sh.A.A, made contributions to the laboratory work. Z.F.A and S.S.M analyzed data. Z.F.A authored the manuscript, with contributions from Z.V and S.S.M in the process of revising it. F.N have contribution to made GSs and was an adviser in this study. M.S and H.N supervised the study.

Funding

All the support and funding from the Research Council of Tarbiat Modares University.
(TMU), Tehran, Iran.

Data availability

The datasets that were used and analyzed in this study could be obtained by contacting the corresponding author and will be promptly provided upon request.

Declarations

Ethics approval and consent to participate

Dr. Farhood Najafi of the Institute for Color Science and Technology's Department of Resin and Additives in Tehran, Iran, found and confirmed GSs. Curcumin with a purity of 99.5% is used as traditional medicine and is available from the Institute of Color Science and Technology. Tamoxifen citrate provided from Sigma-Aldrich Company in St. Louis, MO, USA, and the study was carried out in conformity with ethical guidelines and regulations.

Consent for publication

Not applicable.

Clinical trial number

Not applicable.

Competing interests

The authors declare no competing interests.

Author details

[1]Department of Nanobiotechnology, Faculty of Biological Science, Tarbiat Modares University, Tehran, Iran
[2]ATMP Department, Breast Cancer Research Center, Motamed Cancer Institute, ACECR, Tehran, Iran
[3]Department of Bioactive Compounds, Faculty of Interdisciplinary Sciences and Technologies, Tarbiat Modares University, Tehran, Iran
[4]Department of Resin and Additives, Institute for Color Science and Technology, Tehran, Iran
[5]Department of Physics, Shahid Beheshti University, Tehran, Iran
[6]Department of Molecular Genetics, Faculty of Biological Sciences, Tarbiat Modares University, Tehran, Iran

Received: 28 November 2023 / Accepted: 3 September 2024
Published online: 20 September 2024

References

1. Sung H, et al. Global Cancer statistics 2020: GLOBOCAN estimates of incidence and Mortality Worldwide for 36 cancers in 185 countries. CA Cancer J Clin. 2021;71(3):209–49.
2. Ali S, et al. Molecular mechanisms and mode of tamoxifen resistance in breast cancer. Bioinformation. 2016;12(3):135–9.
3. Sani A et al. Revolutionizing anticancer drug delivery: exploring the potential of tamoxifen-loaded nanoformulations. J Drug Deliv Sci Technol, 2023: p. 104642.
4. Mortazavi SMR, et al. A novel cerasomal gallic acid as a non-ulcerogenic agent with an improved anti-inflammatory potential. J Drug Deliv Sci Technol. 2023;86:104610.

5. Vaezi Z, et al. Hemoglobin bio-adhesive nanoparticles as a colon-specific delivery system for sustained release of 5-aminosalicylic acid in the effective treatment of inflammatory bowel disease. Int J Pharm. 2022;616:121531.
6. Sadeghi Mohammadi S, Vaezi Z, Naderi-Manesh H. Improvement of anti-biofilm activities via co-delivery of curcumin and gentamicin in lipid-polymer hybrid nanoparticle. J Biomater Sci Polym Ed. 2022;33(2):174–96.
7. Christfort JF, et al. Sequential drug release achieved with dual-compartment microcontainers: toward combination therapy. Adv Ther. 2022;5(11):2200106.
8. Rahimzadeh M, et al. Application of a novel pH-responsive gemini surfactant for delivery of curcumin molecules. Mater Res Express. 2020;7(6):065403.
9. Huang F, et al. Micelles based on Acid Degradable Poly(acetal urethane): Preparation, pH-Sensitivity, and triggered intracellular drug release. Biomacromolecules. 2015;16(7):2228–36.
10. Luo W, et al. Microwave/ultrasound-assisted modification of montmorillonite by conventional and gemini alkyl quaternary ammonium salts for adsorption of chromate and phenol: structure-function relationship. Sci Total Environ. 2019;655:1104–12.
11. Pulido-Moran M, et al. Curcumin Health Molecules. 2016;21(3):264.
12. Cai F-Y, et al. Enhanced antitumour efficacy of functionalized doxorubicin plus schisandrin B co-delivery liposomes via inhibiting epithelial-mesenchymal transition. J Liposome Res. 2021;31(2):113–29.
13. Zhai B, et al. Molecular targets of β-elemene, a herbal extract used in traditional Chinese medicine, and its potential role in cancer therapy: a review. Biomed Pharmacother. 2019;114:108812.
14. Zhan XK, et al. Betulinic acid exerts potent antitumor effects on paclitaxel–resistant human lung carcinoma cells (H460) via G2/M phase cell cycle arrest and induction of mitochondrial apoptosis. Oncol Lett. 2018;16(3):3628–34.
15. Zhang X et al. *Quercetin enhanced paclitaxel therapeutic effects towards PC-3 prostate cancer through ER stress induction and ROS production.* OncoTargets and therapy, 2020: pp. 513–523.
16. Rolta R, et al. Bioassay guided Fractionation of Phytocompounds from Bergenia Ligulata: a synergistic approach to treat drug resistant bacterial and fungal pathogens. Pharmacol Research-Modern Chin Med. 2022;3:100076.
17. Mehta J, Rolta R, Dev K. Role of medicinal plants from North Western Himalayas as an efflux pump inhibitor against MDR AcrAB-TolC Salmonella enterica serovar typhimurium: in vitro and in silico studies. J Ethnopharmacol. 2022;282:114589.
18. Pakizehkar S, et al. Curcumin loaded PEG400-OA nanoparticles: a suitable system to increase apoptosis, decrease migration, and deregulate miR-125b/miR182 in MDA-MB-231 human breast cancer cells. Polym Adv Technol. 2020;31(8):1793–804.
19. Verma SP, Goldin BR, Lin PS. The inhibition of the estrogenic effects of pesticides and environmental chemicals by curcumin and isoflavonoids. Environ Health Perspect. 1998;106(12):807–12.
20. Sinha R, et al. Nanotechnology in cancer therapeutics: bioconjugated nanoparticles for drug delivery. Mol Cancer Ther. 2006;5(8):1909–17.
21. Peyvand P, et al. Imidazolium-based ionic liquid functionalized mesoporous silica nanoparticles as a promising nano-carrier: response surface strategy to investigate and optimize loading and release process for Lapatinib delivery. Pharm Dev Technol. 2020;25(9):1150–61.
22. Rahnama S, et al. Milk thistle nano-micelle formulation promotes cell cycle arrest and apoptosis in hepatocellular carcinoma cells through modulating miR-155-3p/SOCS2/PHLDA1 signaling axis. BMC Complement Med Ther. 2023;23(1):337.
23. Gou M, et al. Curcumin-loaded biodegradable polymeric micelles for colon cancer therapy in vitro and in vivo. Nanoscale. 2011;3(4):1558–67.
24. Qi C, et al. Co-delivery of curcumin and capsaicin by dual-targeting liposomes for inhibition of aHSC-induced drug resistance and metastasis. ACS Appl Mater Interfaces. 2021;13(14):16019–35.
25. Albert E, Shirosaki Y. and c.a. che abdullah, *Drug Release and Kinetic Study of Tamoxifen Citrate conjugated with Magnetite Nanoparticle for Drug Delivery Application*. 2018.
26. Kumar P, Nagarajan A, Uchil PD. Analysis of cell viability by the MTT assay. Cold spring harbor protocols; 2018. 2018(6).
27. Ni W, et al. Dual-targeting nanoparticles: Codelivery of Curcumin and 5-Fluorouracil for synergistic treatment of Hepatocarcinoma. J Pharm Sci. 2019;108(3):1284–95.
28. Hajigholami S, et al. Nano Packaged Tamoxifen and curcumin; effective formulation against sensitive and resistant MCF-7 cells. Iran J Pharm Res. 2018;17(1):1–10.
29. Puri S, et al. Drug incorporation and release of water soluble drugs from novel functionalised poly (glycerol adipate) nanoparticles. J Controlled Release. 2008;125(1):59–67.
30. Jose A, et al. Temperature-sensitive liposomes for co-delivery of tamoxifen and imatinib for synergistic breast cancer treatment. J Liposome Res. 2019;29(2):153–62.
31. Banerjee C, et al. Effect of encapsulation of curcumin in polymeric nanoparticles: how efficient to control ESIPT process? Langmuir. 2014;30(36):10834–44.
32. Mello VAd, Ricci-Júnior E. Encapsulation of naproxen in nanostructured system: structural characterization and in vitro release studies. Quím Nova. 2011;34:933–9.
33. Behbahani ES, et al. Curcumin loaded nanostructured lipid carriers: in vitro digestion and release studies. Polyhedron. 2019;164:113–22.
34. Mukherjee S, et al. Green chemistry approach for the synthesis and stabilization of biocompatible gold nanoparticles and their potential applications in cancer therapy. Nanotechnology. 2012;23(45):455103.
35. Maji R, et al. Preparation and characterization of tamoxifen citrate loaded nanoparticles for breast cancer therapy. Int J Nanomed. 2014;9:3107–18.
36. Cao J, et al. Investigation on the interaction behavior between curcumin and PAMAM dendrimer by spectral and docking studies. Spectrochim Acta Part A Mol Biomol Spectrosc. 2013;108:251–5.
37. van Riel Neto F, et al. Optical spectroscopy study of the interaction between curcumin and acrylic polymers. Spectrochim Acta Part A Mol Biomol Spectrosc. 2021;260:119954.
38. Rapalli VK, et al. UV spectrophotometric method for characterization of curcumin loaded nanostructured lipid nanocarriers in simulated conditions: Method development, in-vitro and ex-vivo applications in topical delivery. Spectrochim Acta Mol Biomol Spectrosc. 2020;224:117392.
39. Ha PT, et al. Preparation and anti-cancer activity of polymer-encapsulated curcumin nanoparticles. Adv Nat Sci NanoSci NanoTechnol. 2012;3(3):035002.
40. Zhu Z, et al. The reversion of anti-cancer drug antagonism of tamoxifen and docetaxel by the hyaluronic acid-decorated polymeric nanoparticles. Pharmacol Res. 2017;126:84–96.
41. Khuroo T, et al. Topotecan-Tamoxifen Duple PLGA polymeric nanoparticles: investigation of in vitro, in vivo and cellular uptake potential. Int J Pharm. 2014;473(1–2):384–94.
42. Raiche-Marcoux G, et al. Parametric Drug Release Optimization of anti-inflammatory drugs by gold nanoparticles for topically Applied Ocular Therapy. Int J Mol Sci. 2022;23(24):16191.
43. Swinney DC. *Molecular mechanism of action (MMoA) in drug discovery*, in *Annual Reports in Medicinal Chemistry*. 2011, Elsevier. pp. 301–317.
44. Cho YA, Lee W, Choi JS. Effects of curcumin on the pharmacokinetics of tamoxifen and its active metabolite, 4-hydroxytamoxifen, in rats: possible role of CYP3A4 and P-glycoprotein inhibition by curcumin. Pharmazie. 2012;67(2):124–30.
45. Mohammadi SS, et al. Chemiluminescent liposomes as a theranostic carrier for detection of tumor cells under oxidative stress. Anal Chim Acta. 2019;1059:113–23.
46. Ibrahim AB, et al. Evaluation of tamoxifen and simvastatin as the combination therapy for the treatment of hormonal dependent breast cancer cells. Toxicol Rep. 2019;6:1114–26.
47. Baghi N, et al. Dendrosomal nanocurcumin and exogenous p53 can act synergistically to elicit anticancer effects on breast cancer cells. Gene. 2018;670:55–62.
48. Atanasov AG, et al. Natural products in drug discovery: advances and opportunities. Nat Rev Drug Discovery. 2021;20(3):200–16.
49. Meena R, et al. Effects of hydroxyapatite nanoparticles on proliferation and apoptosis of human breast cancer cells (MCF-7). J Nanopart Res. 2012;14:1–11.
50. Xu M, et al. Sequential delivery of dual drugs with nanostructured lipid carriers for improving synergistic tumor treatment effect. Drug Delivery. 2020;27(1):983–95.
51. Dang Y-P, et al. Curcumin improves the paclitaxel–induced apoptosis of HPV–positive human cervical cancer cells via the NF–κB–p53–caspase–3 pathway. Experimental Therapeutic Med. 2015;9(4):1470–6.
52. Jiang M, et al. Curcumin induces cell death and restores tamoxifen sensitivity in the antiestrogen-resistant breast cancer cell lines MCF-7/LCC2 and MCF-7/LCC9. Molecules. 2013;18(1):701–20.
53. Cosco D, et al. Gemcitabine and tamoxifen-loaded liposomes as multidrug carriers for the treatment of breast cancer diseases. Int J Pharm. 2012;422(1–2):229–37.

54. Chen S, et al. Co-delivery of curcumin and piperine in zein-carrageenan core-shell nanoparticles: formation, structure, stability and in vitro gastrointestinal digestion. Food Hydrocolloids. 2020;99:105334.
55. Khan MM et al. Co-delivery of curcumin and cisplatin to enhance cytotoxicity of cisplatin using lipid-chitosan hybrid nanoparticles. Int J Nanomed, 2020: pp. 2207–17.
56. Jain AK, Thanki K, Jain S. Co-encapsulation of tamoxifen and quercetin in polymeric nanoparticles: implications on oral bioavailability, antitumor efficacy, and drug-induced toxicity. Mol Pharm. 2013;10(9):3459–74.
57. Champion JA, Katare YK, Mitragotri S. Particle shape: a new design parameter for micro-and nanoscale drug delivery carriers. J Controlled Release. 2007;121(1–2):3–9.
58. Ren J, et al. Particle size and distribution of biodegradable poly-D, L-lactide-co-poly (ethylene glycol) block polymer nanoparticles prepared by nanoprecipitation. J Appl Polym Sci. 2005;98(5):1884–90.
59. Mukherjee B, et al. Preparation, characterization and in-vitro evaluation of sustained release protein-loaded nanoparticles based on biodegradable polymers. Int J Nanomed. 2008;3(4):487–96.
60. Al-Jubori AA, et al. Layer-by-layer nanoparticles of tamoxifen and resveratrol for Dual Drug Delivery System and potential triple-negative breast Cancer Treatment. Pharmaceutics. 2021;13(7):1098.
61. Chou T-C. Drug combination studies and their synergy quantification using the Chou-Talalay method. Cancer Res. 2010;70(2):440–6.
62. Vaezi Z, et al. Investigation of the programmed cell death by encapsulated cytoskeleton drug liposomes using a microfluidic platform. Microfluid Nanofluid. 2020;24:1–15.
63. Khamis AAA, et al. Hesperidin, piperine and bee venom synergistically potentiate the anticancer effect of tamoxifen against breast cancer cells. Biomed Pharmacother. 2018;105:1335–43.
64. Scarano W, de Souza P, Stenzel MH. Dual-drug delivery of curcumin and platinum drugs in polymeric micelles enhances the synergistic effects: a double act for the treatment of multidrug-resistant cancer. Biomater Sci. 2015;3(1):163–74.
65. Elshal M, et al. Concanavalin-A shows synergistic cytotoxicity with tamoxifen via inducing apoptosis in estrogen receptor-positive breast cancer: in vitro and molecular docking studies. Pharm Sci. 2021;28(1):76–85.
66. Zoi V, et al. Curcumin and Radiotherapy exert synergistic Anti-glioma Effect in Vitro. Biomedicines. 2021;9(11):1562.
67. Liu H-T, Ho Y-S. Anticancer effect of curcumin on breast cancer and stem cells. Food Sci Hum Wellness. 2018;7(2):134–7.
68. Farsani SSM, et al. Nanocurcumin as a novel stimulator of megakaryopoiesis that ameliorates chemotherapy-induced thrombocytopenia in mice. Life Sci. 2020;256:117840.
69. Frohlich E. The role of surface charge in cellular uptake and cytotoxicity of medical nanoparticles. Int J Nanomed. 2012;7:5577–91.
70. Xu S, et al. Precise ratiometric co-loading, co-delivery and intracellular co-release of paclitaxel and curcumin by aid of their conjugation to the same gold nanorods to exert synergistic effects on MCF-7/ADR cells. J Drug Deliv Sci Technol. 2019;54:101383.
71. Martínez-Edo G, et al. Glycyrrhetinic acid-functionalized mesoporous silica nanoparticles for the co-delivery of DOX/CPT-PEG for targeting HepG2 cells. Pharmaceutics. 2020;12(11):1048.
72. Gao C, et al. pH-responsive prodrug nanoparticles based on a sodium alginate derivative for selective co-release of doxorubicin and curcumin into tumor cells. Nanoscale. 2017;9(34):12533–42.
73. Yang Z, et al. pH multistage responsive micellar system with charge-switch and PEG layer detachment for co-delivery of paclitaxel and curcumin to synergistically eliminate breast cancer stem cells. Biomaterials. 2017;147:53–67.
74. Makhlouf A, Hajdu I, Badea I. Gemini surfactant-based systems for drug and gene delivery. Organic materials as Smart Nanocarriers for Drug Delivery. Elsevier; 2018. pp. 561–600.

Publisher's note